ACS OMEGA

http://pubs.acs.org/journal/acsodf

Article

Development of the PANI/MWCNT Nanocomposite-Based Fluorescent Sensor for Selective Detection of Aqueous Ammonia

Debasis Maity, Mathankumar Manoharan, and Ramasamy Thangavelu Rajendra Kumar*

Cite This: *ACS Omega* 2020, 5, 8414−8422

Read Online

ACCESS | Metrics & More | Article Recommendations | Supporting Information

ABSTRACT: The present work reported the polyaniline (PANI) and multiwalled carbon nanotube (MWCNT)-based nanocomposite as a sensing material for the determination of aqueous ammonia by the enhanced fluorescence method. The excitation wavelength-dependent photoluminescence (PL) intensity has shown dual emission peaks at 340 and 380 nm that correspond to two different excitation energy states. The pH-based PL intensity and zeta potential variation were analyzed to optimize the suitable medium for aqueous ammonia sensing. Zeta potential was found to shift from 4 to −21 mV upon changing the pH of the the solution from acidic to alkaline medium. The fluorescence intensity of PANI/MWCNTs was found to increase upon increasing the pH from 3.0 to 6.0 (acidic region) and exhibits a plateau upon further increasing the pH from 7.0 to 12 (basic region). The PANI/MWCNT composite has shown a linear response to aqueous ammonia concentration varying from 25 to 200 μM with a correlation coefficient (R^2) of 0.99 and a limit of detection of 15.19 μM. The presence of relevant interference molecules and physiological ions had no influence on the detection of aqueous ammonia. Field-level study demonstrated that the level of aqueous ammonia can be determined selectively by using the PANI/MWCNT composite for various applications. The mechanism for the selective detection of aqueous ammonia is deliberated in detail.

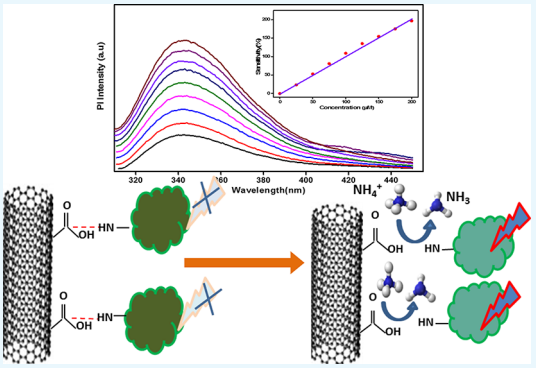

1. INTRODUCTION

Ammonia has a very significant role in the global ecosystem, specifically in the nitrogen cycle. However, excess emissions of ammonia from domestic, industrial, and agricultural wastewater to the aquatic environment can cause water eutrophication and damage ecosystems, leading to algae flourishing and aquatic organism poisoning. If we concern about aquatic life, plants have more limited tolerance for aqueous ammonia compared with animals (fish, insect, etc.).

The large amount of ammonia that is needed or more than permissible limit affects their growth and structural development, and it can affect their tissues (gills), leading to skin, kidney, and liver damage that increase the possibility of death. The long period of time consumption of aqueous ammonia affects the metabolism and acid−base equilibrium of body, concerning the glucose tolerance level in the body and also the reducing tissue sensitivity to insulin. The ammonium level in the blood of healthy adults and children is approximately 30 μM, but these levels can be exceeded to 1 mM under conditions of acute hyperammonemia (1−3 mM). The toxicity of aqueous ammonia depends on both temperature and the pH value of water. The allowed range of aqueous ammonia in drinking water was from 14.04 to 640.44 μM.[1]

Therefore, prevention and control of ammonia pollution by monitoring dissolved ammonia in the environment are significantly important for the environment where it can directly accumulate and damage the aquatic life. The commonly used methods (amperometric, resistive) to quantify the aqueous ammonia for environmental, industrial, and biomedical purposes are cost-effective and time-consuming.[2−5] The recently fluorescence-based detection system has been developed using various nanomaterials such as polymer nanoparticles and quantum dots because of their ultrasensitivity, rapidness, lower cost, higher portability, and easy operations.[6,7] Fluorometric systems have been successfully used for sensing gaseous analyte molecules.

Carbon nanotubes are one of the most important one-dimensional nanomaterials due to its excellent electrical, mechanical, and physical properties.[8,9] The polymer composites, metal, metal oxide decoration, and different functional groups were introduced in carbon nanotubes to improve selectivity and sensitivity for various applications.[10−13] PANI is a very important conducting polymer, which is being investigated in recent years due to its low cost, nontoxicity, reversibility, good environmental stability, and high intrinsic redox properties.[14] Generally, the carbon nanotube/PANI

Received: September 5, 2019
Accepted: March 26, 2020
Published: April 10, 2020

https://dx.doi.org/10.1021/acsomega.9b02885
ACS Omega 2020, 5, 8414−8422

composite was studied for its unique optical, electrical, and electrochemical properties.[15−19]

The determination of aqueous ammonia has the potential for water quality monitoring, environmental safety, and biomedical diagnostic applications. The commonly used methods to quantify the ammonia in blood are alkalization−diffusion,[5] ion exchange,[20] and enzymatic reactions[21] and use gas sensing electrodes, which involve a complex operation procedure, are less stable, and have poor selectivity. Most of the demonstrated methods for detecting ammonia in the aqueous medium lack selectivity and require combination of extraction and analyzing processes. Therefore, we require a compact, portable, ultrasensitive, rapid, lower cost, and simple operation strategy-based method for the detection of ammonia in aqueous solutions. As per our knowledge so far, no report is available on PANI/MWCNT-based aqueous ammonia detection.There are many reports existing for the detection of ammonia; however, the detection of aqueous ammonia is rare. The fluorescence properties of PANI were rarely used for the sensing application. Here, we demonstrate the detection of aqueous ammonia by measuring the change in fluorescence of the PANI/MWCNT nanocomposite. The nanocomposite was formulated by using the amine group of PANI that has an affinity toward the carboxyl group on the MWCNTs. The physical properties of the sample were characterized by using scanning electron microscopy, ultraviolet−visible absorption, zeta potential, and spectrofluorometry. The optical properties of the nanocomposite were investigated in different pH values and at different excitation wavelengths. The sensing methodology was well evaluated by introducing various possible interferences, and the sensing mechanism is elucidated in detail.

2. EXPERIMENTAL SECTIONS

2.1. Materials and Reagents. Carboxyl-functionalized MWCNTs were synthesized by the single-step pyrolysis method using the tubular furnace at 870 °C. The characterization and properties were already reported in our previous articles.[22−24] Liquor aqueous ammonia, lactose, lysine, sucrose, uric acid, zinc chloride, sodium chloride, potassium chloride, calcium chloride, magnesium chloride, glucose, succinic acid, disodium phosphate, and potassium monophosphate were purchased from Sigma-Aldrich. Phosphate buffer solution (0.1 M, pH 7.4 during sensing) and ultrapure water (18.2 MΩ cm at 25 °C) were used throughout the experiment.

2.2. Formation of Carboxyl-Functionalized MWCNTs and PANI Nanocomposite. Carboxyl-functionalized MWCNTs were prepared by acid treatment to remove the unwanted catalyst. To prepare PANI, 0.1 M ammonium disulfate was dropwise added in HCl, which contains 0.1 M aniline solution, and it was kept for 12 h at room temperature. The deep green color of polyaniline was formed by a chemical oxidation process that was purified by centrifugation at 8000 rpm for 10 min. The nanocomposite formulation was optimized by varying the PANI concentrations (100, 20, and 10 mg/mL) with 1 mg/mL MWCNTs in an aqueous medium. The samples were defined as S_P1 (100:1), S_P2 (20:1), and S_P3 (10:1) throughout the experiment. The mixture was stirred for 30 min and followed by probe sonication for 10 min for the formation of the nanocomposite. From the characterization, the combination of 10 mg/mL PANI and 1 mg/mL MWCNTs has formed a suitable nanocomposite as anticipated, and it was used for further sensing studies (PBS, pH 7.4). The synthesis process is shown in Figure 1.

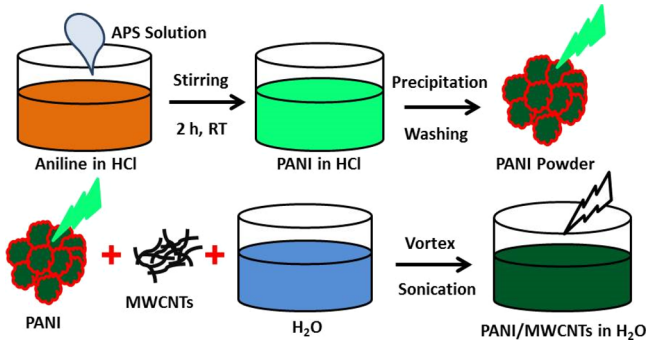

Figure 1. Schematic representation of the synthesis of the PANI/MWCNT composite.

2.3. Instrumentation. SEM images were taken by an FEI QUANTA 200 instrument using a 30 kV beam under vacuum. The structure and morphology were examined using high-resolution transmission electron microscopy (JEOL JEM-2010, HRTEM, Japan) in-built with selected area (electron) diffraction (SAED). X-ray diffraction (XRD) measurement was performed by an X'pert Pro diffractometer with Cu Kα radiation in the range $5 < 2\theta < 80$ at 40 kV. Raman spectra were obtained using an Ar ion laser (514 nm, HORIBA Jobin Yvon). Thermogravimetric analysis (TGA) was done using an STA 6000 SaturnA sensor. Emission spectra and sensing studies were performed using a spectrofluorometer (HORIBA Jobin Yvon FluroMax-4). Zeta potential was measured by a zetasizer Malvern. Absorbance spectra were taken using a UV−visible spectrophotometer (UV-VIS3600, Shimadzu). Emission spectra and sensing studies were performed using spectrofluorometer (HORIBA Jobin Yvon FluroMax-4).

3. RESULTS AND DISCUSSION

3.1. Morphological Observation. The microstructure and morphology of MWCNTs and PANI/MWCNTs were studied by SEM (Figure S1). MWCNTs have a denser network with 0.1−5 μm in length (Figure S1a). Figure S1b shows the granular morphology of PANI. The average diameter of PANI was 0.5 μm, which helps the formation of the nanocomposite. The carbon nanotube is properly embedded in the PANI matrix due to interfacial bonding between MWCNTs and the PANI matrix. The greater amount of PANI totally covers MWCNTs and forms the PANI/MWCNT composite (Figure S1c).

Figure 2a−c shows HRTEM images of the PANI composite under different magnifications. The aggregation of the MWCNT network in the polymer matrix was observed (Figure S2a−d). The diameter and length distribution of synthesized close-ended (Figure S2) MWCNTs are about 40 nm and a length of 0.2 to 1.6 mm, respectively, with an inner gap and wall thickness around 8 and 16 nm, respectively.[24,25] The selected area (electron) diffraction pattern (SAED) of PANI/MWCNTs gives three rings corresponding to (002), (100), and (004) planes of MWCNTs (Figure 2d).

3.2. X-ray Diffraction (XRD) Analysis. Figure 3a displays the X-ray diffraction (XRD) pattern of MWCNTs, PANI, and PANI/MWCNTs. MWCNTs show well-defined peaks at 26.10, 43.68, 53.78, and 78.11° (2θ) those correspond to the

https://dx.doi.org/10.1021/acsomega.9b02885
ACS Omega 2020, 5, 8414−8422

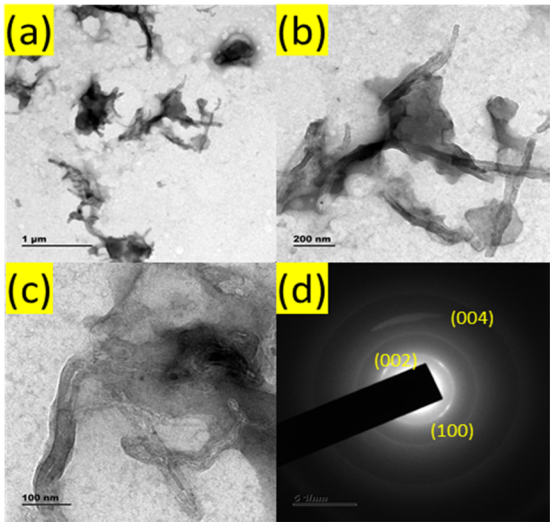

Figure 2. (a–c) HRTEM images of the PANI/MWCNT nanocomposite and (d) corresponding SAED pattern.

(002), (101), (004), and (110) planes of MWCNTs, respectively, and they are well matched with JCPDS card nos. 75-1621 and 41-1487.[25] The spectra of PANI show lower crystalline peaks at 25.50° that corresponds to the (200) plane due to periodicity perpendicular to the polymer chain, which is similar to HCl-doped PANI XRD patterns.[26−29] The PANI/MWCNT composite shows crystallinity peaks of both MWCNTs and PANI.

3.3. Raman Analysis. Raman spectroscopy is a well-known method of characterization to check configuration, purity, and crystallinity of MWCNTs. Raman peaks were observed at 1350, 1580, and 2700 cm^{-1} due to the disordered D band, the degree of graphitization of the G band, and phonon resonance of the G′ band.[30] The calculated I_D/I_G ratio from the Raman spectrum of MWCNTs is 0.498. The Raman spectra of PANI at 1579,1476, and 1330 cm^{-1} are due to C═C of the quinoid rings from PANI where 1397 and 1180 cm^{-1} are due to the branch structure of PANI with tertiary nitrogen groups.[31,32] The C═C of quinoid of PANI and the G band of MWCNTs were superposed each other. The intensity of G and 2D peaks was reduced due to the coverage of PANI on MWCNTs.

3.4. Thermogravimetric Analysis. The thermal stability of MWCNTs, PANI, and the PANI/MWCNT nanocomposite was analyzed by thermogravimetric analysis in 20 mL/min N_2 atmosphere, as shown in Figure 3c. MWCNTs have shown a single-step weight loss process beyond 600 °C due to the well graphitic structure of the nanotubes. The TGA curve of PANI shows weight loss at a lower temperature due to its moisture content. The major weight loss at 350−600 °C is due to the decomposition process of PANI. However, the slow weight loss was observed for the PANI/MWCNT composite up to 350 °C that was due to the loss of co-intercalated water molecules and the release of co-intercalated HCl. The decomposition of the PANI/MWCNTs occurs at 400 to 600 °C (50%) that might be associated with the decomposition of amine-based groups of PANI, and remaining weight loss was due to oxygenated groups of MWCNTs those have not reacted with an amine. It was observed that the major weight loss of the PANI/MWCNT starts at 400 °C, which occurs earlier than that of the MWCNTs.

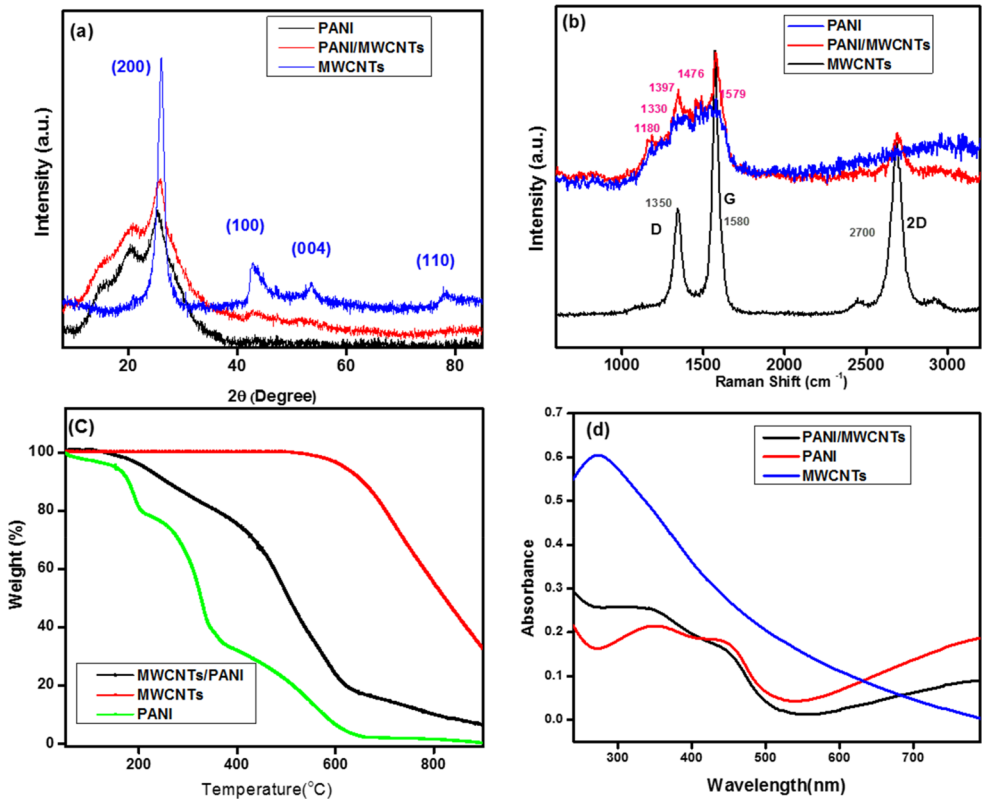

Figure 3. (a) X-ray diffraction pattern, (b) Raman analysis, (c) TGA analysis, and (d) UV−Vis spectrum of the prepared MWCNTs, PANI, and PANI/MWCNTs.

https://dx.doi.org/10.1021/acsomega.9b02885
ACS Omega 2020, 5, 8414−8422

3.5. Optical Properties. The UV−vis spectrum (Figure 3d) of the carboxyl-functionalized MWCNTs shows a strong absorbance band at 273 nm. The chemically synthesized PANI has two absorbance peaks at 343 and 442 nm due to polaron $n-\pi^*$ transition of benzenoid rings and polaron$-\pi^*$ transition, respectively.[33,34] The optical absorption spectra of the PANI/MWCNT nanocomposite sample show an increase in absorption at 273 nm, and two characteristic absorbance peaks (343 and 442 nm) indicate the presence of both MWCNTs and PANI.

3.6. Fluorescence Properties of PANI/MWCNTs. The photoluminescence spectra of PANI/MWCNTs were measured at different excitation wavelengths (250−350 nm) those have given the emission in the range of 300−500 nm (Figure 4). The bi emission spectra were observed at 344 and 380 nm based on excitation wavelengths.

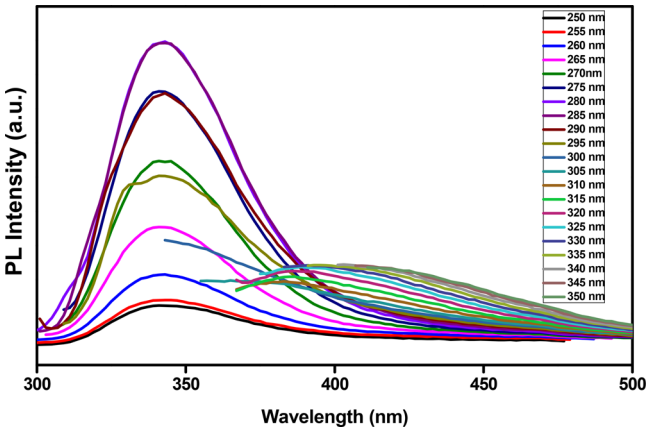

Figure 4. Photoluminescence spectra of the PANI/MWCNT composite.

The first emission peak at 340 nm was due to the $\pi-\pi^*$ transition of a benzenoid unit of PANI. The emission peak positions have not shown peak shifting, but the intensity was gradually increased with excitation wavelength up to 285 nm. The second emission peak was observed at 380 nm when excitation wavelength goes beyond 300 nm due to lighter dopant chlorine ions in PANI that is from HCl.

3.7. pH-Dependent PL Intensity and Zeta Potential. The pH-dependent PL intensity of the PANI/MWCNT composite was investigated in the wide range of pH in phosphate buffer solution, as shown in Figure 5a,b. Intrinsic inhomogeneity and the electronic structure of PANI/MWCNT composites led to different PL intensities depend on pH and excitation wavelength.[35,36]

The maximum intensity was observed at 340 nm in the range of 6−7 pH. The fluorescence intensity of PANI/MWCNTs was found to increase upon increasing the pH from 3.0 to 6.0 and exhibits a plateau upon further increasing the pH from 7.0 to 12. The pH-dependent PL property of the PANI/MWCNTs may be attributed to the protonation of the amino groups of PANI surfaces.[37] Protonation (by H^+ ions) of PANI results in a decrease in the PL intensity of PANI. At acidic medium (pH 3), the degree of protonation of PANI is higher due to the presence of larger number of background H^+ ions, which results in a lower PL intensity of PANI/MWCNT composites. Upon increasing the pH from 3 to 7, the background H^+ ions reduced, thereby decreasing the degree of protonation of PANI results in an increase in the PL intensity of PANI. Also, the background H^+ drastically decreases upon further increasing the pH from 7 to 13, which reduces the probability of protonation, and thus, there is no change in the PL intensity observed in the basic medium.

The zeta potential of PANI/MWCNT was found to vary from 5 to −21 mV that corresponds to the change in the pH (3−12) of the medium, as shown in Figure 5b. The isoelectric point was observed at pH 3.5. The highly negative surface charge was maintained in an alkaline medium and helps to prevent the agglomeration. Based on the results, it can be concluded that the pH 7.4 and an excitation wavelength of 285 nm that gives a high PL intensity at 345 nm were found to be optimum for sensing applications.

3.8. Aqueous Ammonia Sensing Performance of PANI/MWCNTs. Fluorescence-based aqueous ammonia sensing by the PANI/MWCNT composite is shown in Figure 5c,d. From the 3D contour plot, it was observed that the PL intensity has been increased sharply around 500% in the presence of 0.5 mM aqueous ammonia. The PL emission intensity was shown as the Gaussian maximum at 340 nm when excited by 285 nm at pH 7.4 in phosphate buffer solution. The fluorescence spectra of PANI/MWCNT composites are shown in Figure 6 upon the addition of different concentrations of aqueous ammonia (500 μM). There was neither a shift in the emission peak nor change in full width at half-maximum in the presence of aqueous ammonia. The PL intensity of PANI/MWCNTs has linearly increased in the presence of aqueous ammonia concentration ranges from 0 to 200 μM in phosphate buffer solution.

The normalized PL intensity of the sample is calculated from the measured change in the intensity in the presence of a solution (F_a) and initial PL intensity value (F_b) using eq 1

$$\text{sensitivity}\%(S) = \frac{F_a - F_b}{F_b} \times 100 \quad (1)$$

The PL intensity was increased linearly in the presence of different concentrations of aqueous ammonia (Figure 6). The slope values of S_p1, S_p2, and S_p3 samples were 0.126, 1.000, and 0.091, respectively. For S_p1, S_p2, and S_p3 composite samples, the correlation coefficients were found to be 0.995, 0.994, and 0.991, respectively. The lower detection limit values (LOD S/N = 3) for samples S_p1, S_p2, and S_p3 were 14.70, 15.19, and 18.57 μM, respectively. It was observed that there is a significant alteration in the limit of detection (LOD) and PL intensity when there is an increment in PANI percentage in a composite.

The increase in the PL intensity is due to the breaking of PANI/MWCNT bonding by delocalization of trapped charge carriers in the presence of NH_4^+. The available PANI/MWCNT interface associated with the samples (S_p1, S_p2, and S_p3) is important for the change in the observed PL intensity. The slope has almost nine times enhancement for the S_p2 sample when compared to the higher and lower concentrations of PANI in composites S_p1 and S_p3. This significant enhancement indicates that the S_p2 composite has higher sensitivity than other composites in the presence of the same amount of aqueous ammonia. The fraction of PANI/MWCNTs in the samples are given by S_p1 (100:1), S_p2 (20:1), and S_p3 (10:1), and this is evident from the corresponding PL intensities. However, the sample S_p2 shows a larger change in fluorescence due to the availability

https://dx.doi.org/10.1021/acsomega.9b02885
ACS Omega 2020, 5, 8414−8422

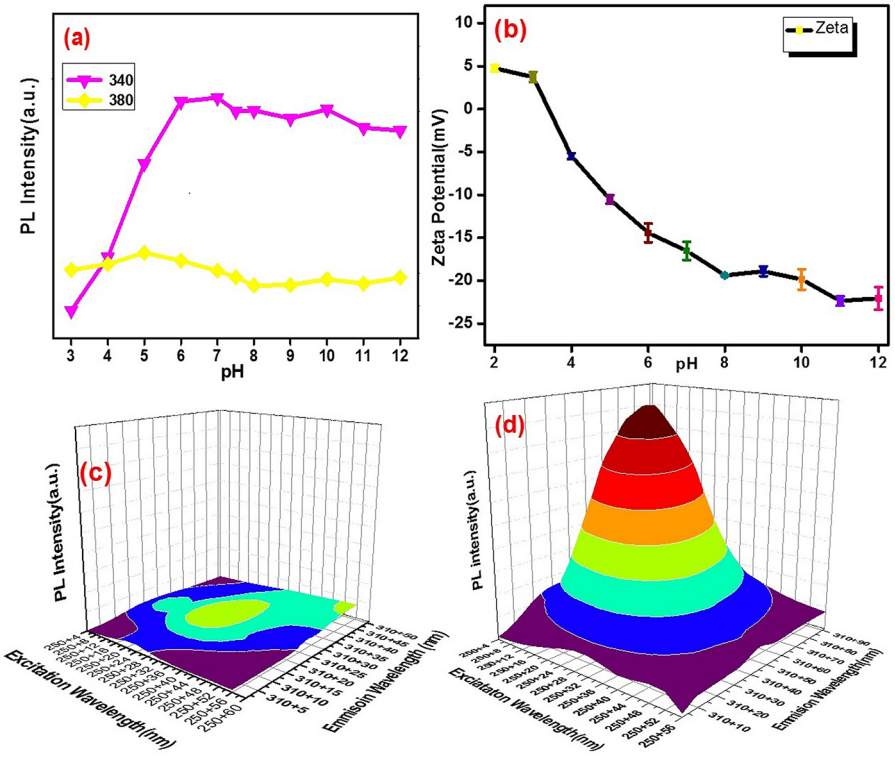

Figure 5. (a) pH-dependent and (b) zeta potential-dependent PL intensity of the PANI/MWCNT composite. (c, d) Emission spectra of PANI/MWCNT composites at pH 7.4 (3D contour plot) at different excitation wavelengths in the (c) absence of aqueous ammonia and (d) presence of aqueous ammonia.

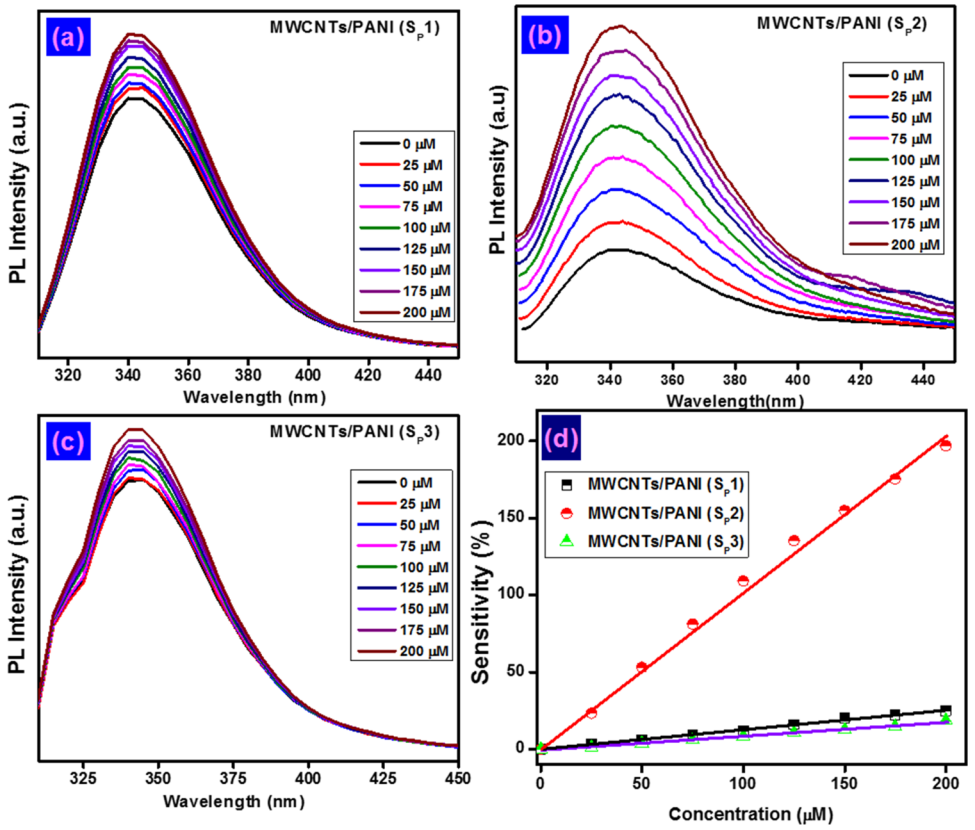

Figure 6. (a–c) Fluorescence spectra of samples (a) S_P1, (b) S_P2, and (c) S_P3 at different concentrations of aqueous ammonia. (d) Calibrated linear fit graph of aqueous ammonia sensing with different weight ratios of MWCNTs and PANI (S_P1, S_P2, and S_P3).

https://dx.doi.org/10.1021/acsomega.9b02885
ACS Omega 2020, 5, 8414−8422

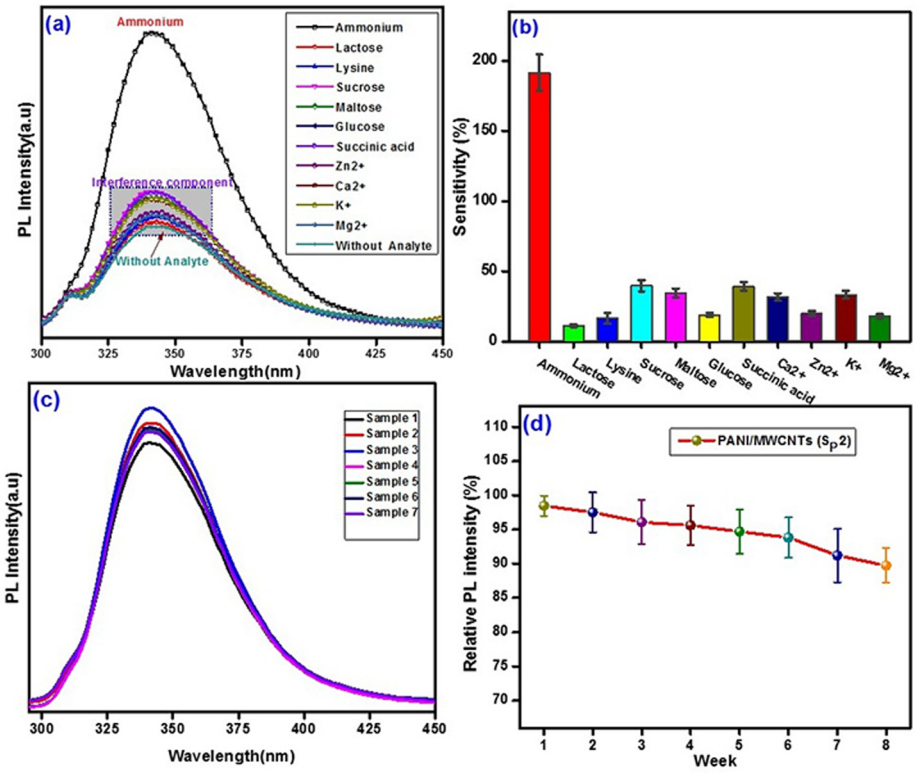

Figure 7. (a) PL spectra and (b) calibration of the PANI/MWCNT-based ammonium sensor against relevant interference. (c) Reproducibility of ammonium sensing for seven different samples and (d) stability of the PANI/MWCNT composite.

of relatively larger area of the PANI/MWCNT interface. The sample S_p1 contains large fraction of PANI (100 times) compared to MWCNTs, which might result in covering most of MWCNTs, and leaves a very measurable area of the PANI/MWCNT interface for ammonia sensing. In the case of S_p3, it posseses very less fraction of PANI and results in less number of PANI/MWCNT interface sites for ammonia sensing. A moderate amount of PANI/MWCNTs (20:1) in S_p2 allows the exposure of larger area of the PANI/MWCNT interface for ammonia, which could results in a higher change in the PL intensity, in other words, higher sensitivity. It can be concluded that the proper composition of each compound of a composite could make an efficient sensor platform for liquid aqueous ammonia.

3.9. Selectivity and Stability Study. It was observed from Figure 8 that the PL intensity of the PANI/MWCNT composite was increased to 200% in the presence of 200 μM aqueous ammonia.

The selectivity of the sensor was analyzed with the following possible interferences such as lactose, lysine, sucrose, maltose, Zn^{2+}, Ca^{2+}, K^{+}, Mg^{2+}, glucose, and succinic acid. All the interference compounds were taken an equal amount of ammonium (200 μM). Figure 7a,b shows that the interference molecules have a negligible impact toward the detection of aqueous ammonia. From this study, it can be concluded that the PANI/MWCNT composite has high selectivity and can be applied to the direct determination of aqueous ammonia in field-level samples. Further, we investigate the reproducibility of ammonium sensing performance of the PANI/MWCNT sensor, as shown in Figure 7c. The sensor shows excellent reproducibility with a 6.37 standard deviation for seven sets of the sample in the presence of 200 μM aqueous ammonia. The stability of the composite was analyzed up to 8 weeks of continuous measurement (Figure 7d). The PL intensity of the PANI/MWCNT nanocomposite decreased by about 10.3% after 8 weeks, where only 1.6% change was observed for first week.

3.10. On Field Evaluation of Developed Sensing Methodology. Field applicability of the developed fluorescent nanocomposites was evaluated by detecting aqueous ammonia in human serum. The ammonium level in the blood of a healthy human is approximately 30 μM, and in hyperammonemia condition, it may exceed to 1 mM. The experimental results obtained by the standard addition method in dilute human plasma are shown in Table 1. The recovery experiments were carried out as a preliminary evaluation to illustrate the real application. The recovery percentage range was obtained 92 to 96 with less than 7 relative standard deviations, indicating an acceptable level of accuracy of our proposed sensor.

Table 1. Detection of Aqueous Ammonium in Human Serum

sample	spike (μM)	found (nm)	recovery	% RSD (n = 3)
human serum	40	37.12	92.80	5.93
	60	56.62	94.36	5.93
	80	74.67	93.33	3.12
	100	96.34	96.34	6.93
	200	191.03	95.15	2.34

3.11. Mechanism of Sensing. The fluorescence off-to-on mechanism of the PANI/MWCNT composite probe for the detection of aqueous ammonia is represented in Figure 8. The interactions between PANI and carboxyl-functionalized carbon nanotubes take place due to the electrostatic interaction

https://dx.doi.org/10.1021/acsomega.9b02885
ACS Omega 2020, 5, 8414−8422

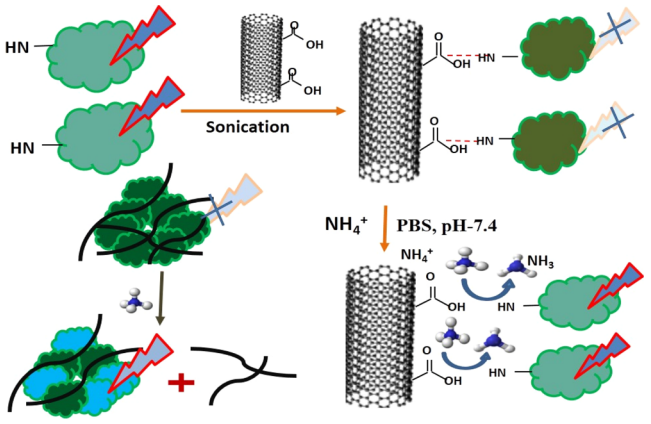

Figure 8. Mechanism of aqueous ammonia sensing by the PANI/MWCNTs composite.

between $-COO^-$ groups of carbon nanotubes and $-NH^+$ of PANI, the hydrogen bonding between −OH groups on the carbon nanotubes and the −NH group of PANI, and also a small amount of $-\pi$ stacking between the π-bonded of the carbon nanotube and the quinoid ring of PANI.[38−41] Due to the bonding formation of the PANI/MWCNTs complex, the fluorescence efficiency of PANI was effectively quenched by localization or trapping of charge carrier (Figure S3).

The aqueous ammonia (NH_4^+) donated a proton to PANI and delocalized the trapped charged carrier again to restore the fluorescence of PANI. This resulted in the sensitive and selective detection of aqueous ammonia by measuring the change in the fluorescence properties.[42]

Although there are a large number of literature reports available for the detection of gaseous phase sensing of ammonia, there is a research gap for the detection of aqueous ammonia. The detection of aqueous ammonia has potential for water quality monitoring and environmental safety concern. Most of the literature has not covered elaborated information about the effect of pH and selectivity, and as per our knowledge so far, no report is available based on PANI/MWCNTs for the detection of aqueous ammonia. Comparative study of available literature report is listed in Table 2. It is clear that our aqueous ammonia detection protocol was compact and has a systematic investigation when compared to other literature. These results suggest that PANI/MWCNT-based new fluorescence sensing methodology would be beneficial in the detection of aqueous ammonia for various applications.

4. CONCLUSIONS

This study successfully demonstrated the novel approach for sensing of aqueous ammonia by the PANI/MWCNT composite through fluorescence methods. The characteristic features of the PANI/MWCNT composite were studied by using scanning electron microscopy (SEM), high-resolution transmission electron microscopy (HRTEM), ultraviolet−visible absorption (UV), zeta potential, and spectrofluorometry. The pH-based PL intensity analysis was helpful to optimize an exact pH for aqueous ammonia sensing. The optimization of various concentrations of PANI to formulate a nanocomposite was an appealing factor to elevate the sensing performance. The developed sensing platform was highly sensitive and selective toward aqueous ammonia among the pool of possible interferences. The linear responses for different concentrations of aqueous ammonia range from 25 to 200 μM with a high correlation coefficient (R^2 = 0.99) and an LOD of 15.19 μM by the nanocomposite gave a platform for the sensitive detection of diseases in real sample analysis. The composite stability under UV exposure for a longer duration of period and the possible mechanism of sensing were clearly elucidated in detail. This PANI/MWCNT composite is free of metal organic dyes, cost-effective, and easily reproducible. The present approach had extended a new path for the selective and sensitive detection of aqueous ammonia, which is essential in the biomedical, environmental monitoring, and chemical industry fields.

■ ASSOCIATED CONTENT

Supporting Information

The Supporting Information is available free of charge at https://pubs.acs.org/doi/10.1021/acsomega.9b02885.

SEM image and HRTEM image of the PANI/MWCNT nanocomposite and PL spectra of PANI, the PANI/MWCNT composite, and the PANI/MWCNT composite with the presence of ammonia (PDF)

■ AUTHOR INFORMATION

Corresponding Author

Ramasamy Thangavelu Rajendra Kumar − *Department of NanoScience and Technology, Bharathiar University, Coimbatore 641046, Tamil Nadu, India;* orcid.org/0000-0002-4188-5859; Email: rtrkumar@buc.edu.in

Authors

Debasis Maity − *DRDO-BU Center for Life Sciences, Bharathiar University, Coimbatore 641046, India*

Mathankumar Manoharan − *Department of NanoScience and Technology, Bharathiar University, Coimbatore 641046, Tamil Nadu, India*

Complete contact information is available at: https://pubs.acs.org/10.1021/acsomega.9b02885

Table 2. Comparison Table of Aqueous Ammonia Detection from Literature Report

sensing materials	detection methods	detection range	LOD	interference study	ref
LCW	fluorescence	0−60 mM	35 μM		43
PANI	impedance	0−200 μM	25 μM		3
Ag NCs	fluorescence	10−350 μM	3.20 μM	yes	44
CDs	fluorescence	1.75−12.24 mM	105 μM		7
aza-BODIPY dyes	fluorescence	0−8.56 μM	3 nM		45
polyaniline	optical	0.35−14.0 mM			46
PANI/MWCNTs	fluorescence	25−200 μM	15.19 μM	yes	our work

https://dx.doi.org/10.1021/acsomega.9b02885
ACS Omega 2020, 5, 8414−8422

Notes

The authors declare no competing financial interest.

■ ACKNOWLEDGMENTS

This research work is financially supported by the Defence Research and Development Organisation (DRDO), New Delhi, Govt of India (grant no.DLS/86/50011/DRDO-BU center/1748/D (R&D). DRDO-BU Center for Life Sciences, Bharathiar University for providing the equipment facility for experiments is also being acknowledged.

■ REFERENCES

(1) Barsotti, R. J. Measurement of Ammonia in Blood. *J. Pediatr.* **2001**, *138*, S11.
(2) Azmi, N. E.; Abdullah, J.; Ahmad, M.; Sidek, H.; Heng, L. Y.; Rahman, S. A. An Optical Based Biosensor for the Determination of Ammonium in Aqueous Environment. *Am. J. Anal. Chem.* **2012**, *03*, 364−370.
(3) Brannelly, N. T.; Killard, A. J. A Printed and Microfabricated Sensor Device for the Sensitive Low Volume Measurement of Aqueous Ammonia. *Electroanalysis* **2017**, *29*, 162−171.
(4) Brannelly, N. T.; Killard, A. J. An Electrochemical Sensor Device for Measuring Blood Ammonia at the Point of Care. *Talanta* **2017**, *167*, 296−301.
(5) Ayyub, O. B.; Behrens, A. M.; Heligman, B. T.; Natoli, M. E.; Ayoub, J. J.; Cunningham, G.; Summar, M.; Kofinas, P. Simple and Inexpensive Quantification of Ammonia in Whole Blood. *Mol. Genet. Metab.* **2015**, *115*, 95−100.
(6) Zhang, X.; Zhu, Y.; Li, X.; Guo, X.; Zhang, B.; Jia, X.; Dai, B. A Simple, Fast and Low-Cost Turn-on Fluorescence Method for Dopamine Detection Using in Situ Reaction. *Anal. Chim. Acta* **2016**, *944*, 51−56.
(7) Ganiga, M.; Cyriac, J. FRET based ammonia sensor using carbon dots. *Sens Actuators, B Chem.* **2016**, *225*, 522−528.
(8) Lieber, C. M. One-Dimensional Nanostructures: Chemistry, Physics & Applications. *Solid State Commun.* **1998**, *107*, 607−616.
(9) Baughman, R. H.; Zakhidov, A. A.; de Heer, W. A. Carbon Nanotubes–the Route Toward Applications. *Science* **2002**, *297*, 787−792.
(10) Balasubramanian, K.; Burghard, M. Chemically Functionalized Carbon Nanotubes. *Small* **2005**, *1*, 180−192.
(11) Li, C.; Thostenson, E. T.; Chou, T.-W. Sensors and Actuators Based on Carbon Nanotubes and Their Composites: A Review. *Compos. Sci. Technol.* **2008**, *68*, 1227−1249.
(12) Maity, D.; Minitha, C. R.; Rajendra Kumar, R. T. Glucose Oxidase Immobilized Amine Terminated Multiwall Carbon Nanotubes/Reduced Graphene Oxide/Polyaniline/Gold Nanoparticles Modified Screen-Printed Carbon Electrode for Highly Sensitive Amperometric Glucose Detection. *Mater. Sci. Eng. C* **2019**, *105*, 110075.
(13) Maity, D.; Rajendra Kumar, R. T. Highly Sensitive Amperometric Detection of Glutamate by Glutamic Oxidase Immobilized Pt Nanoparticle Decorated Multiwalled Carbon Nanotubes(MWCNTs)/Polypyrrole Composite. *Biosens. Bioelectron.* **2019**, *130*, 307.
(14) Liu, T.; Finn, L.; Yu, M.; Wang, H.; Zhai, T.; Lu, X.; Tong, Y.; Li, Y. Polyaniline and Polypyrrole Pseudocapacitor Electrodes with Excellent Cycling Stability. *Nano Lett.* **2014**, *14*, 2522−2527.
(15) Zhou, Z.; Wu, X.-F.; Hou, H. Electrospun Carbon Nanofibers Surface-Grown with Carbon Nanotubes and Polyaniline for Use as High-Performance Electrode Materials of Supercapacitors. *RSC Adv.* **2014**, *4*, 23622−23629.
(16) Xiao, Y.; Lin, J.-Y.; Wu, J.; Tai, S.-Y.; Yue, G.; Lin, T.-W. Dye-Sensitized Solar Cells with High-Performance Polyaniline/Multi-Wall Carbon Nanotube Counter Electrodes Electropolymerized by a Pulse Potentiostatic Technique. *J. Power Sources* **2013**, *233*, 320−325.
(17) Singh, R.; Dhand, C.; Sumana, G.; Verma, R.; Sood, S.; Gupta, R. K.; Malhotra, B. D. Polyaniline/Carbon Nanotubes Platform for Sexually Transmitted Disease Detection. *J. Mol. Recognit.* **2010**, *23*, 472−479.
(18) Tran, L. D.; Nguyen, D. T.; Nguyen, B. H.; Do, Q. P.; Le Nguyen, H. Development of Interdigitated Arrays Coated with Functional Polyaniline/MWCNT for Electrochemical Biodetection: Application for Human Papilloma Virus. *Talanta* **2011**, *85*, 1560−1565.
(19) Nabid, M. R.; Sedghi, R.; Sharifi, R.; Oskooie, H. A.; Heravi, M. M. Removal of Toxic Nitrate Ions from Drinking Water Using Conducting Polymer/MWCNTs Nanocomposites. *Iran. Polym. J.* **2013**, *22*, 85−92.
(20) Mori, M.; Tanaka, K.; Helaleh, M. I. H.; Xu, Q.; Ikedo, M.; Ogura, Y.; Sato, S.; Hu, W.; Hasebe, K. Selective Determination of Ammonium Ions by High-Speed Ion-Exclusion Chromatography on a Weakly Basic Anion-Exchange Resin Column. *J. Chromatogr. A* **2003**, *997*, 191−197.
(21) Miller, E. F.; Maier, R. J. Ammonium Metabolism Enzymes Aid Helicobacter Pylori Acid Resistance. *J. Bacteriol.* **2014**, *196*, 3074−3081.
(22) Maity, D.; Rajavel, K.; Rajendra Kumar, R. T. Polyvinyl Alcohol Wrapped Multiwall Carbon Nanotube (MWCNTs) Network on Fabrics for Wearable Room Temperature Ethanol Sensor. *Sens. Actuators, B* **2018**, *261*, 297−306.
(23) Maity, D.; Kumar, R. T. R. Polyaniline Anchored MWCNTs on Fabric for High Performance Wearable Ammonia Sensor. *ACS Sensors* **2018**, *3*, 1822−1830.
(24) Rajavel, K.; Dinesh, M.; Saranya, R.; Rajendra Kumar, R. T. Enhanced Vacuum Sensing Performance of Multiwalled Carbon Nanotubes: Role of Defects And Carboxyl Functionalization. *RSC Adv.* **2015**, *5*, 20479−20485.
(25) Rajavel, K.; Lalitha, M.; Radhakrishnan, J. K.; Senthilkumar, L.; Rajendra Kumar, R. T. Multiwalled Carbon Nanotube Oxygen Sensor: Enhanced Oxygen Sensitivity at Room Temperature and Mechanism of Sensing. *ACS Appl. Mater. Interfaces* **2015**, *7*, 23857−23865.
(26) Morsi, R. E.; Elsabee, M. Z. Polyaniline Nanotubes: Mercury and Competative Heavy Metals Uptake. *Am. J. Polym. Sci.* **2015**, *5*, 5923.
(27) Yan, J.; Wei, T.; Fan, Z.; Qian, W.; Zhang, M.; Shen, X.; Wei, F. Preparation of Graphene Nanosheet/Carbon Nanotube/Polyaniline Composite as Electrode Material for Supercapacitors. *J. Power Sources* **2010**, *195*, 3041−3045.
(28) Kondawar, S. B.; Deshpande, M. D.; Agrawal, S. P. Transport Properties of Conductive Polyaniline Nanocomposites Based on Carbon Nanotubes. *Int. J. Compos. Mater.* **2012**, *2*, 32−36.
(29) Xu, H.; Zhang, J.; Chen, Y.; Lu, H.; Zhuang, J. Electrochemical Polymerization of Polyaniline Doped with Zn2+as the Electrode Material for Electrochemical Supercapacitors. *J. Solid State Electrochem.* **2014**, *18*, 813−819.
(30) Wang, Z.; Liu, E.; Gu, D.; Wang, Y. Glassy Carbon Electrode Coated with Polyaniline-Functionalized Carbon Nanotubes for Detection of Trace Lead in Acetate Solution. *Thin Solid Films* **2011**, *519*, 5280−5284.
(31) Shakoor, A.; Rizvi, T. Z. Raman Spectroscopy of Conducting Poly (Methyl Methacrylate)/Polyaniline Dodecylbenzenesulfonate Blends. *J. Raman Spectrosc.* **2010**, *41*, 237−240.
(32) Wang, L.; Yao, Q.; Bi, H.; Huang, F.; Wang, Q.; Chen, L. PANI/Graphene Nanocomposite Films with High Thermoelectric Properties by Enhanced Molecular Ordering. *J. Mater. Chem. A* **2015**, *3*, 7086−7092.
(33) Bhattacharya, P.; Dhibar, S.; Hatui, G.; Mandal, A.; Das, T.; Das, C. K. Graphene Decorated with Hexagonal Shaped M-Type Ferrite and Polyaniline Wrapper: A Potential Candidate for Electromagnetic Wave Absorbing and Energy Storage Device Applications. *RSC Adv.* **2014**, *4*, 17039−17053.
(34) Khalid, M.; Tumelero, M. A.; Pasa, A. A. Asymmetric and Symmetric Solid-State Supercapacitors Based on 3D Interconnected Polyaniline-Carbon Nanotube Framework. *RSC Adv.* **2015**, *5*, 62033−62039.

https://dx.doi.org/10.1021/acsomega.9b02885
ACS Omega 2020, 5, 8414−8422

(35) Dispenza, C.; Sabatino, M. A.; Chmielewska, D.; Lopresti, C.; Battaglia, G. Inherently Fluorescent Polyaniline Nanoparticles in a Dynamic Landscape. *React. Funct. Polym.* **2012**, *72*, 185−197.
(36) Datta, S.; Das, P. K. *Author ' s Accepted Manuscript*; Elsevier: 2016, 138, DOI: 10.1016/j.jlumin.2016.08.068.
(37) Liu, Y.; Ding, Y.; Gou, H.; Huang, X.; Zhang, G.; Zhang, Q.; Liu, Y.; Meng, Z.; Xi, K.; Jia, X. Room Temperature Synthesis of PH-Switchable Polyaniline Quantum Dots as a Turn-on Fluorescent Probe for Acidic Biotarget Labeling. *Nanoscale* **2018**, *10*, 6660−6670.
(38) Choi, H.-J.; Jeon, I.-Y.; Kang, S.-W.; Baek, J.-B. Electrochemical Activity of a Polyaniline/Polyaniline-Grafted Multiwalled Carbon Nanotube Mixture Produced by a Simple Suspension Polymerization. *Electrochim. Acta* **2011**, *56*, 10023−10031.
(39) Mao, Y.; Bao, Y.; Yan, L.; Li, G.; Li, F.; Han, D.; Zhang, X.; Niu, L. PH-Switched Luminescence and Sensing Properties of a Carbon Dot-Polyaniline Composite. *RSC Adv.* **2013**, *3*, 5475−5482.
(40) Bai, H.; Shi, G. Gas Sensors Based on Conducting Polymers. *Sensors* **2007**, *7*, 267−307.
(41) Qiu, G.; Zhu, A.; Zhang, C. Hierarchically Structured Carbon Nanotube-Polyaniline Nanobrushes for Corrosion Protection over a Wide PH Range. *RSC Adv.* **2017**, *7*, 35330−35339.
(42) Wang, X.; Xuan, H.; Zhang, J.; Chen, S.; Zhang, F.; Zou, W. Facile Synthesis of Fluorescent Polyaniline Microspheres and Their Use for the Detection of Mercury Ions. *New J. Chem.* **2015**, *39*, 6261−6266.
(43) Li, J.; Dasgupta, P. K.; Genfa, Z. Transversely Illuminated Liquid Core Waveguide Based Fluorescence Detection: Fluorometric Flow Injection Determination of Aqueous Ammonium/Ammonia. *Talanta* **1999**, *50*, 617−623.
(44) Dong, J. X.; Gao, Z. F.; Zhang, Y.; Li, B. L.; Li, N. B.; Luo, H. Q. A Selective and Sensitive Optical Sensor for Dissolved Ammonia Detection via Agglomeration of Fluorescent Ag Nanoclusters and Temperature Gradient Headspace Single Drop Microextraction. *Biosens. Bioelectron.* **2017**, *91*, 155−161.
(45) Strobl, M.; Walcher, A.; Mayr, T.; Klimant, I.; Borisov, S. M. Trace Ammonia Sensors Based on Fluorescent Near-Infrared-Emitting Aza-BODIPY Dyes. *Anal. Chem.* **2017**, *89*, 2859−2865.
(46) Castrellon-Uribe, J.; Nicho, M. E.; Reyes-Merino, G. Remote Optical Detection of Low Concentrations of Aqueous Ammonia Employing Conductive Polymers of Polyaniline. *Sens Actuators, B* **2009**, *141*, 40−44.

https://dx.doi.org/10.1021/acsomega.9b02885
ACS Omega 2020, 5, 8414−8422